Nuclear Engineering and Technology 48 (2016) 1376–1386

Available online at ScienceDirect

Nuclear Engineering and Technology

journal homepage: www.elsevier.com/locate/net

Original Article

# Effect of Loading Rate on the Fracture Behavior of Nuclear Piping Materials Under Cyclic Loading Conditions

*Jin Weon Kim* [a,*], *Myung Rak Choi* [a], *and Yun Jae Kim* [b]

[a] *Department of Nuclear Engineering, Chosun University, 309 Pilmun-daero, Dong-gu, Gwangju, 61452, Republic of Korea*

[b] *Department of Mechanical Engineering, Korea University, 145 Anam-ro, Seongbuk-Ku, Seoul 136-701, Republic of Korea*

ARTICLE INFO

*Article history:*
Received 12 March 2016
Received in revised form
27 May 2016
Accepted 2 June 2016
Available online 25 June 2016

*Keywords:*
Cyclic Load
Fracture Behavior
Loading Rate Effect
Nuclear Piping Materials
Seismic Condition

ABSTRACT

This study investigated the loading rate effect on the fracture resistance under cyclic loading conditions to understand clearly the fracture behavior of piping materials under seismic conditions. *J*–*R* fracture toughness tests were conducted under monotonic and cyclic loading conditions at various displacement rates at room temperature and the operating temperature of nuclear power plants (i.e., 316°C). SA508 Gr.1a low-alloy steel and SA312 TP316 stainless steel piping materials were used for the tests. The fracture resistance under a reversible cyclic load was considerably lower than that under monotonic load regardless of test temperature, material, and loading rate. Under both cyclic and monotonic loading conditions, the fracture behavior of SA312 TP316 stainless steel was independent of the loading rate at both room temperature and 316°C. For SA508 Gr.1a low-alloy steel, the loading rate effect on the fracture behavior was appreciable at 316°C under cyclic and monotonic loading conditions. However, the loading rate effect diminished when the cyclic load ratio of the load (*R*) was −1. Thus, it was recognized that the fracture behavior of piping materials, including seismic loading characteristics, can be evaluated when tested under a cyclic load of $R = -1$ at a quasistatic loading rate.



## 1. Introduction

Piping components of nuclear power plants (NPPs) are designed and maintained to ensure their structural integrity under seismic and normal operation conditions [1–3]. Interest in the structural integrity of nuclear piping components during a seismic event greatly increased after the nuclear accident at the Fukushima Daiichi NPPs [4]. Thus, the reliability of integrity assessments of piping components under the seismic loading condition is an important issue. In the current integrity assessment procedures [2,5], seismic loading is treated as monotonic and applied once; the mechanical properties

* *Corresponding author.*
E-mail address: jwkim@chosun.ac.kr (J.W. Kim).

http://dx.doi.org/10.1016/j.net.2016.06.006

**Table 1 – Chemical compositions of SA508 Gr.1a low-alloy steel (LAS) and SA312 TP316 stainless steel (SS) piping materials (wt%).**

| Materials | C | Mn | P | S | Si | Ni | Cr | Mo | V | Al | Cu |
|---|---|---|---|---|---|---|---|---|---|---|---|
| SA508 Gr.1a LAS | 0.223 | 1.27 | 0.009 | 0.0047 | 0.225 | 0.242 | 0.118 | 0.026 | 0.003 | 0.024 | 0.200 |
| SA312 TP316 SS | 0.021 | 1.25 | 0.038 | 0.004 | 0.45 | 12.21 | 16.31 | 2.06 | – | – | – |

obtained from the monotonic and quasistatic loading conditions are used for the assessment. However, the seismic load has both dynamic and cyclic characteristics and the mechanical properties under dynamic and cyclic loading conditions are different from those under monotonic and quasistatic loading conditions [6]. Hence, ignoring the dynamic and cyclic loading characteristics in the mechanical properties of piping materials could cause uncertainty in the integrity assessment of piping components under the seismic loading condition.

A number of studies have investigated the cyclic loading effect on the fracture behavior of materials; specifically, the influences of cyclic compressive load level and frequency on the fracture resistance of materials have been evaluated [6–12]. All of these reports showed that the fracture resistance was significantly reduced by reversible cyclic loading when compared to that under monotonic loading, and that the reduction was dependent on the cyclic compressive load level and frequency. Also, they showed that such fracture behavior under cyclic loading was attributable to fatigue and a fracture synergy that accelerated crack extension. However, most of the investigations were based on cyclic tests at a quasistatic loading rate rather than at a dynamic loading rate [7–12]. Only a few studies have performed cyclic fracture tests under the dynamic loading condition and they reported that the interaction between cyclic and dynamic loading effects was negligible. Thus, both effects on the fracture behavior can be considered separately [6]. However, this conclusion was drawn from only a very limited test condition, i.e., a single dynamic loading rate; the loading rate under the seismic loading condition depends on the routing of the piping system and the location within the piping components. In particular, the deformation rate near the crack-tip, which is closely related to the loading rate and directly affects the fracture behavior of materials, is more difficult to quantify under the seismic loading condition because it depends on the geometry and location of the crack within the piping components. Considering such uncertainty in the loading rate under the seismic condition, it is necessary to investigate the loading rate effect on the fracture behavior of materials under the cyclic loading condition to clearly understand the fracture behavior of piping components under the seismic condition.

Therefore, this study conducted $J$–$R$ fracture toughness testing of two piping materials commonly used in NPPs under monotonic and cyclic loading conditions at various displacement rates at room temperature (RT) and at the operating temperature of NPPs (316°C). The loading rate effect on the fracture behavior was investigated under monotonic and cyclic loading conditions by comparing the $J$–$R$ curves for different displacement rates. Additionally, appropriate consideration of seismic loading characteristics in the evaluation of the fracture behavior of piping materials is suggested on the basis of these investigations.

## 2. Materials and methods

### 2.1. Test materials and specimens

The piping materials used for these experiments were SA508 Gr.1a low-alloy steel (LAS) and SA312 TP316 stainless steel (SS). SA508 Gr.1a LAS is used for main coolant pipelines in Korean Standard NPPs and its dimensions are 1,075.4 mm in outer diameter ($D_o$) and 102.6 mm in thickness ($t$). SA312 TP316 SS is also commonly used for pipelines in the primary system of NPPs (4 inch Schedule 160; $D_o$ = 114.3 mm and $t$ = 13.5 mm). SA508 Gr.1a LAS piping material was normalized at 920°C for 10 minutes and water-quenched, followed by tempering at 650°C for 180 minutes, and SA312 TP316 SS was annealed at 1,040°C and water-quenched. The chemical compositions of both pipe materials are listed in Table 1 and their tensile properties at RT and 316°C under a quasistatic loading rate are summarized in Table 2.

In this study, the fracture resistance of the piping materials was evaluated using compact tension (CT) specimens; a 25.4-mm-thick CT specimen of 1T planar dimension was used for SA508 Gr.1a LAS and a 10.6-mm-thick CT specimen of 0.5T planar dimension was used for SA312 TP316 SS. Both kinds of specimen were designed in accordance with the ASTM E1820–09 standard [13] (Fig. 1) and were machined in the L–C direction, i.e., the notch was oriented in the circumferential direction. All specimens were precracked to a crack length ($a$) of 0.59W, where W is the width of the specimen, and side-grooved on both sides following the ASTM E1820–09 standard [13].

### 2.2. Experimental procedures

#### 2.2.1. Test conditions

$J$–$R$ fracture toughness tests were conducted under both monotonic and cyclic loading conditions at RT and 316°C. Four different displacement rates ($V_{LL}$) were considered in the monotonic tests, i.e., $V_{LL}$ = 0.9 mm/min, 9.0 mm/min, 90 mm/

**Table 2 – Tensile properties of SA508 Gr.1a low-alloy steel (LAS) and SA312 TP316 stainless steel (SS) piping materials under quasistatic loading rate ($\dot{\varepsilon} = 3.95 \times 10^{-4}$/s).**

| Materials | Temp. (°C) | YS (MPa) | UTS (MPa) | TE (%) | RA (%) |
|---|---|---|---|---|---|
| SA508 | RT | 359.9 | 543.6 | 35.9 | 74.8 |
| Gr.1a LAS | 316 | 232.4 | 537.4 | 32.8 | 71.8 |
| SA312 | RT | 266.1 | 573.1 | 66.8 | 82.8 |
| TP316 SS | 316 | 155.2 | 452.5 | 42.3 | 79.6 |

RA, reduction in area; RT, room temperature; TE, total elongation; UTS, ultimate tensile strength; YS, yield stress.

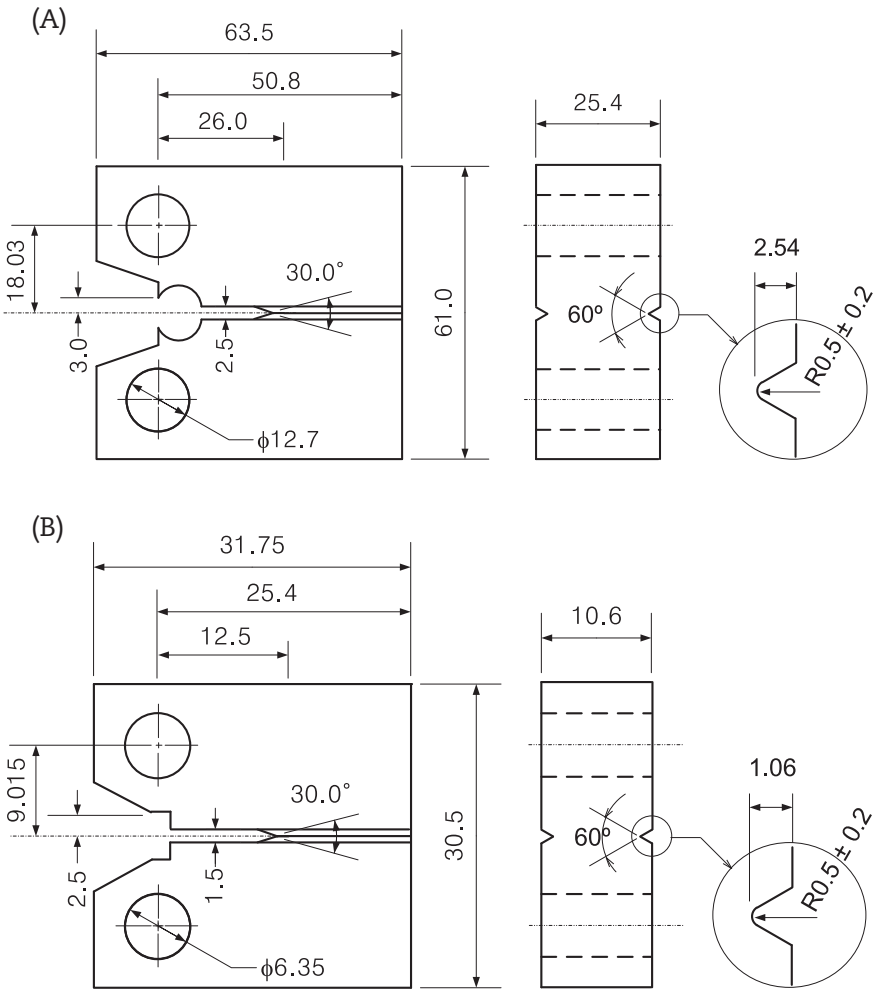


**Fig. 1 – Compact tension (CT) specimens used for *J*–*R* fracture toughness tests. (A) 1T–CT. (B) 0.5T–CT.**

min, and 2,280 mm/min for SA508 Gr.1a LAS and $V_{LL}$ = 0.45 mm/min, 4.5 mm/min, 45 mm/min, and 1,140 mm/min for SA312 TP316 SS. In the cyclic tests, $V_{LL}$ = 0.9 mm/min, 9.0 mm/min, 90 mm/min, and 2,280 mm/min were used for SA508 Gr.1a LAS and $V_{LL}$ = 0.45 mm/min and 45 mm/min for SA312 TP316 SS. The displacement rates of 0.45 mm/min and 0.9 mm/min corresponded to a quasistatic loading rate, and $V_{LL}$ = 1,140 mm/min and 2,280 mm/min corresponded to a typical dynamic loading rate. Lower displacement rates were applied to SA312 TP316 SS compared to SA508 Gr.1a LAS because a smaller specimen was used for the *J*–*R* tests on SA312 TP316 SS. The displacement rates for dynamic *J*–*R* tests were determined using Eq. (1), which was proposed to evaluate the fracture toughness at seismic loading rate in the procedure for leak-before-break evaluation [14].

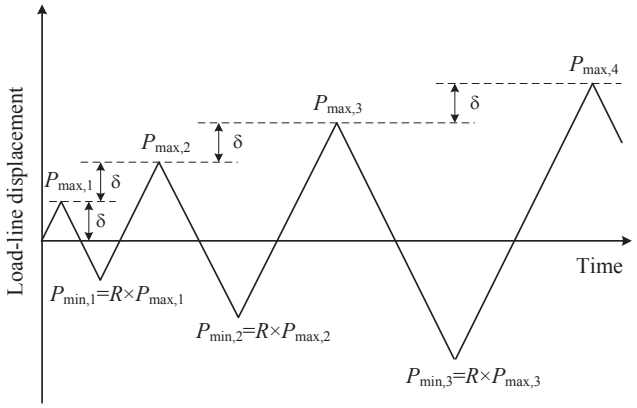


**Fig. 2 – Cyclic loading sequence applied for cyclic *J*–*R* fracture toughness tests. δ, incremental displacement; $P_{min}$, applied load while unloading; R, load ratio ($P_{min}/P_{max}$).**

$$V_{LL} = 4 \times f_1 \times d_i \quad (1)$$

In Eq. (1), $f_1$ is the first mode natural frequency of the piping system and $d_i$ is the load-line displacement (*LLD*) at crack initiation under quasistatic loading condition. In general, a loading rate under seismic condition is considered to be 1,000–10,000 times faster than that typically used for a quasistatic *J*–*R* fracture test [14]. Thus, it is believed the displacement rates of 1,140 mm/min and 2,280 mm/min are appropriate to evaluate the fracture behavior of piping materials under the seismic loading condition.

For monotonic *J*–*R* tests, a tensile displacement was monotonically applied to the specimens without unloading. For cyclic *J*–*R* tests, an incremental displacement-controlled cyclic load was applied following the loading sequence

**Table 3 – Test conditions considered in the experiment.**

| Materials | Loading type | Test temperature (°C) | Cyclic load ratio (R) | Displacement increment (δ, mm) | Load-line displacement rate ($V_{LL}$; mm/min) |
|---|---|---|---|---|---|
| SA508 | Monotonic | RT | N/A | N/A | 0.9, 9.0, 90, 2,280 |
| Gr.1a LAS | | 316 | N/A | N/A | 0.9, 9.0, 90, 2,280 |
| | Cyclic | RT | −0.5 | 0.15 | 0.9, 9.0, 2,280 |
| | | | −1.0 | 0.15 | 0.9, 9.0, 2,280 |
| | | 316 | −0.5 | 0.15 | 0.9, 9.0, 90, 2,280 |
| | | | −1.0 | 0.15 | 0.9, 9.0, 90, 2,280 |
| SA312 | Monotonic | RT | N/A | N/A | 0.45, 4.5, 45, 1,140 |
| TP316 SS | | 316 | N/A | N/A | 0.45, 4.5, 45, 1,140 |
| | Cyclic | RT | −0.5 | 0.15 | 0.45 |
| | | | −1.0 | 0.15 | 0.45, 45 |
| | | 316 | −0.5 | 0.15 | 0.45 |
| | | | −1.0 | 0.15 | 0.45, 45 |

RT, room temperature.

shown in Fig. 2. In the cyclic loading sequence, the displacement was controlled during the tensile loading step, while the load was controlled during the compressive loading step to maintain a constant cyclic load ratio ($R = P_{min}/P_{max}$). In the tests, a constant displacement increment (δ) of 0.15 mm was applied after each cycle and cyclic load ratios of $R = -0.5$ and −1.0 were used. According to the results of previous cyclic *J*–*R*

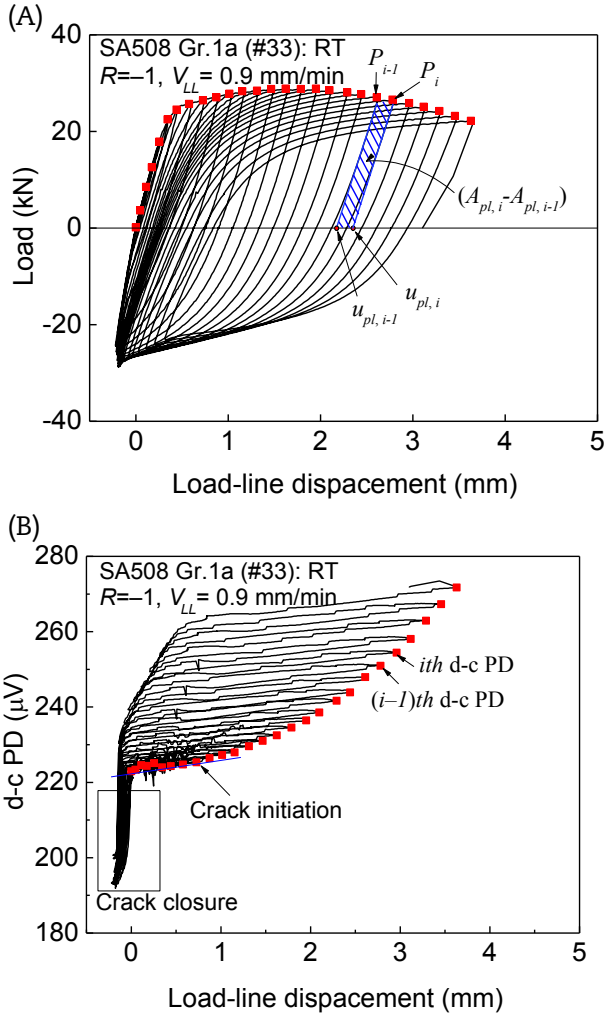


**Fig. 3 – Sample data of a cyclic *J*–*R* fracture toughness test. (A) Load vs. load–line displacement (*LLD*) curve. (B) Direct-current potential drop (d-c PD) vs. *LLD* curve. RT, room temperature.**

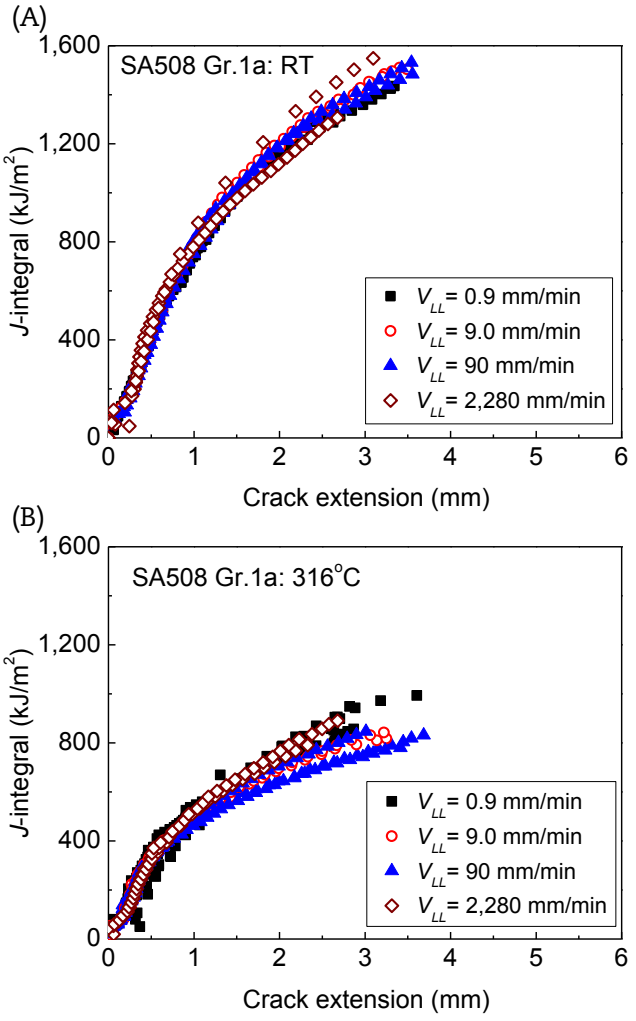


**Fig. 4 – Variation in monotonic *J*–*R* curves of SA508 Gr.1a low-alloy steel (LAS) piping material at different displacement rates. (A) Room temperature. (B) 316°C.**

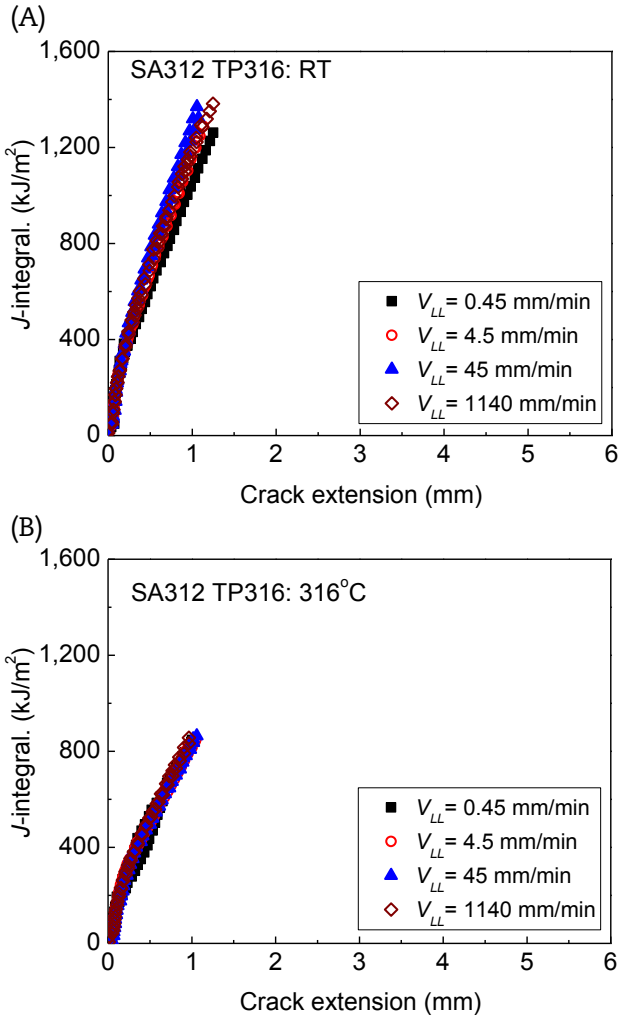


**Fig. 5 – Variation in monotonic *J*–*R* curves of SA312 TP316 stainless steel (SS) piping material at different displacement rates. (A) Room temperature. (B) 316°C.**

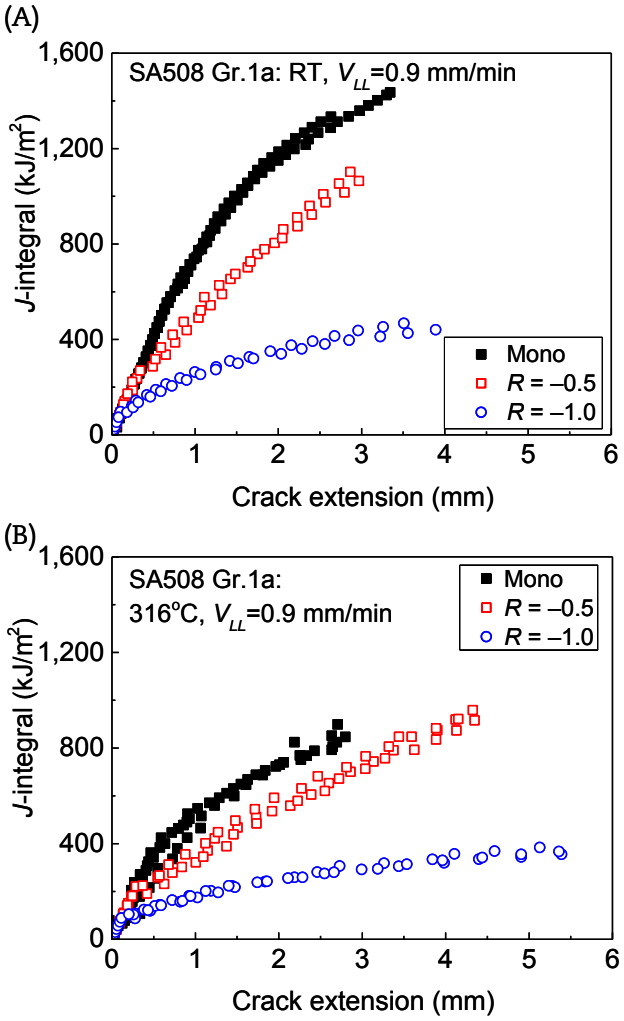


**Fig. 6 – Comparison of *J*–*R* curves of SA508 Gr.1a LAS piping material under monotonic and cyclic loading conditions. (A) Room temperature. (B) 316°C.**

tests, the fracture behavior was strongly dependent on the cyclic load ratio and displacement increment; the more negative the cyclic load ratio or the smaller the displacement increment, the greater the reduction in fracture resistance from cyclic loading [6–8,10–12]. Thus, the displacement increment of 0.15 mm and load ratios of −0.5 and −1.0 were determined from the test conditions that clearly showed the cyclic effect on fracture behavior of materials in the previous studies. Table 3 summarizes the conditions used for *J*–*R* fracture tests in the present study.

### 2.2.2. *Test methods*

In the monotonic *J*–*R* tests, crack extension was determined by the normalization method defined in the ASTM E1820–09 standard [13] and the *J*-integral was calculated in accordance with the standard procedure [13]. Crack extension in the cyclic tests was determined by a direct-current potential drop (d-c PD) method incorporating Johnson's equation [15]. Thus, the load, *LLD*, and d-c PD data were acquired during the cyclic tests. Fig. 3 shows a sample load versus *LLD* curve and a d-c PD vs. *LLD* curve obtained from a cyclic *J*–*R* test.

Unlike the monotonic *J*–*R* test, a standard procedure for evaluating the fracture toughness under a cyclic loading condition is not available. Some studies calculated the *J*-integral from the area under the load vs. *LLD* curve and above the crack opening load [9,16,17]. Others considered that the cyclic *J*–*R* test was a special case of monotonic *J*–*R* test, which was employed to estimate how a monotonic *J*–*R* curve is modified due to cyclic loading, and they calculated the *J*-integral from the envelope area under the load vs. *LLD* curve and above zero load, ignoring the compressive loading portion, in accordance with the ASTM standard procedure [6–8,10–12]. In the present study, the second method was used to obtain the *J*–*R* curve under a cyclic loading condition; i.e., the *J*-integral at each cycle was calculated by Eq. (2) given in the ASTM E1820–09 standard [13]:

$$J_i = \frac{K_i^2(1-\upsilon^2)}{E} + J_{pl,i} \tag{2}$$

where $K_i$, $\upsilon$, and $E$ are the stress intensity factor corresponding to the *i*th loading step, Poisson's ratio, and elastic modulus, respectively, and:

$$J_{pl,i} = \left[J_{pl,i-1} + \left(\frac{\eta_{i-1}}{b_{i-1}}\right)\left(\frac{A_{pl,i} - A_{pl,i-1}}{B_N}\right)\right] \times \left[1 - \gamma_{i-1}\left(\frac{a_i - a_{i-1}}{b_{i-1}}\right)\right] \quad (3)$$

where $a_i$ is instantaneous crack length in the ith loading step that was determined from the ith d-c PD data indicated in Fig. 3B, $b_i$ is uncracked ligament in the ith loading step, $B_N$ is net thickness of specimen, and $\eta_{i-1}$ and $\gamma_{i-1}$ are defined as Eqs. (4) and (5), respectively.

$$\eta_{i-1} = 2 + 0.522\frac{b_{i-1}}{W} \quad (4)$$

$$\gamma_{i-1} = 1 + 0.76\frac{b_{i-1}}{W} \quad (5)$$

In Eq. (3), $A_{pl,i}$ is a plastic area under the envelop curve above zero load for the ith loading step and was calculated by Eq. (6):

$$A_{pl,i} = A_{pl,i-1} + \frac{(P_i + P_{i-1})(u_{pl,i} - u_{pl,i-1})}{2} \quad (6)$$

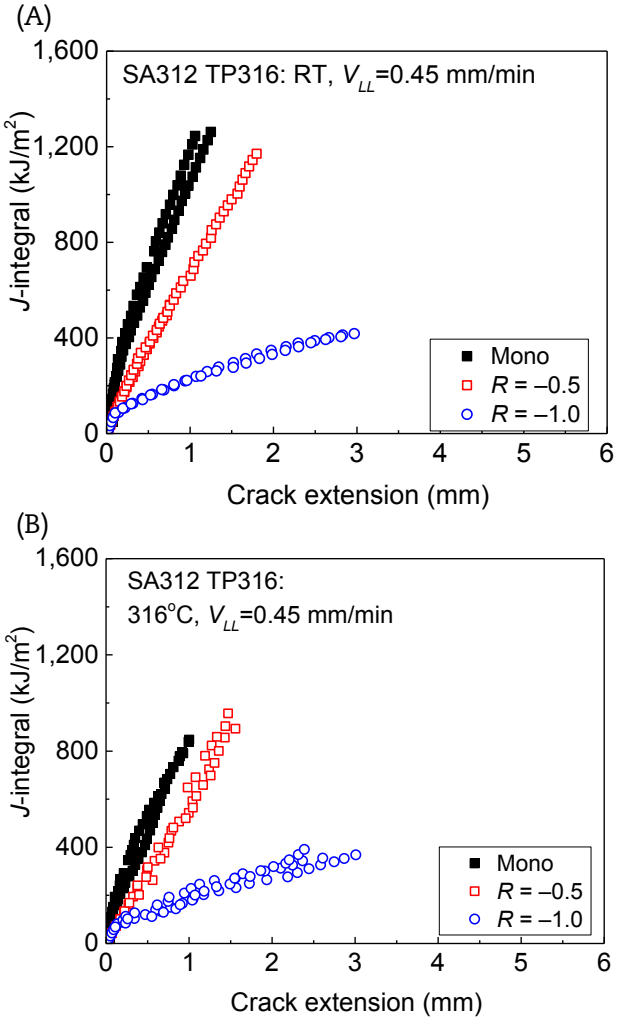


**Fig. 7 – Comparison of J–R curves of SA312 TP316 SS piping material under monotonic and cyclic loading conditions. (A) Room temperature. (B) 316°C.**

where $p_i$ and $u_{pl,i}$ are peak load and plastic part of *LLD* in the ith loading step, respectively, as indicated in Fig. 3A.

All of the tests were conducted using a servo-hydraulic universal testing machine with a 100-kN load cell and a high-temperature furnace. *LLD* was measured using a high-temperature crack opening displacement gauge with a travel length of 10 mm. In the tests at 316°C, the temperature of the specimen was measured and controlled within ± 2°C using K-type thermocouples attached to both sides of the specimen.

## 3. Results and discussion

### 3.1. Monotonic loading condition

Prior to cyclic J–R fracture toughness tests, monotonic J–R tests were conducted at RT and 316°C under various displacement rates to obtain reference J–R curves for each displacement rate and to investigate the loading rate effect on the fracture behavior for both pipe materials under monotonic loading conditions. Fig. 4 exhibits the monotonic J–R curves of SA508 Gr.1a LAS piping material at different displacement

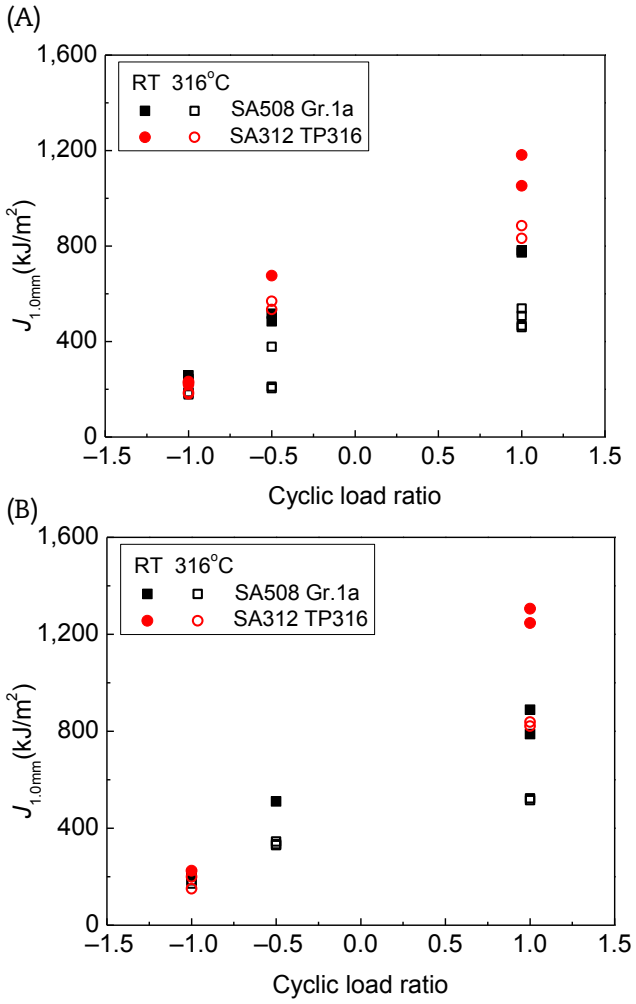


**Fig. 8 – $J_{1.0\ mm}$ values as a function of load ratio for both pipe materials at room temperature (RT) and 316°C. (A) Quasistatic. (B) Dynamic.**

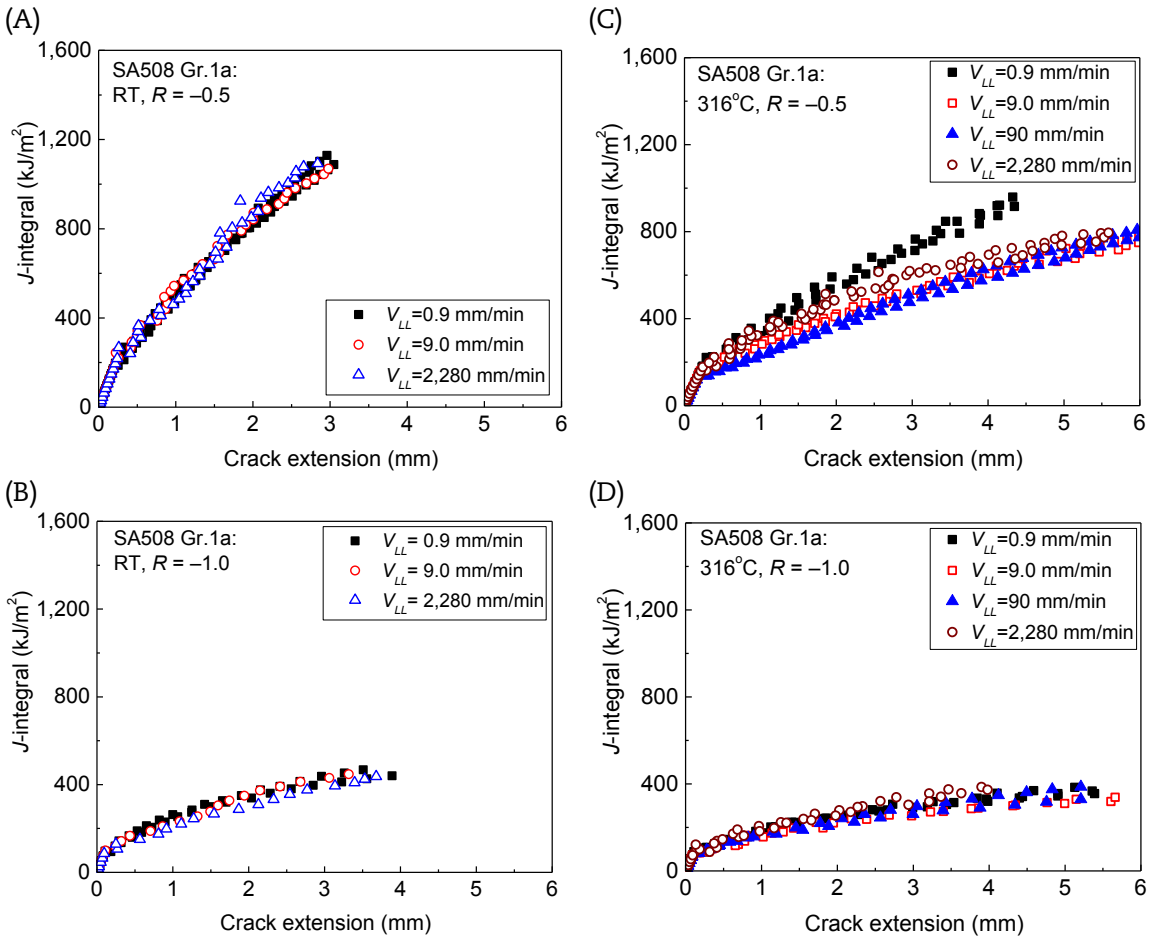


**Fig. 9 – Variation in cyclic J–R curves of SA508 Gr.1a LAS piping material at different displacement rates. (A) Room temperature, R = −0.5. (B) Room temperature, R = −1.0. (C) 316°C, R = −0.5. (D) 316°C, R = −1.0.**

rates at RT and 316°C. Fig. 4A shows that the J–R curves at RT were almost identical, although some scattering was observed at $V_{LL}$ = 2,280 mm/min. However, the variation in J–R curves with displacement rate was appreciable at 316°C (Fig. 4B); the J–R curve decreased with increasing displacement rate and reached a minimum at $V_{LL}$ = 9.0–90 mm/min and then it increased with a further increase in displacement rate. Thus, the J–R curve at the dynamic loading rate ($V_{LL}$ = 2,280 mm/min) was almost the same as that at the quasistatic loading rate ($V_{LL}$ = 0.9 mm/min). Our previous study showed that SA508 Gr.1a LAS piping material was susceptible to dynamic strain aging (DSA) at 316°C and the DSA effect on mechanical properties was most significant in the range of displacement rates of 9.0–90 mm/min [18]. It is well-known that the occurrence of DSA in ferritic steels reduces their fracture resistance at elevated temperatures [19–21]. Therefore, the appearance of a minimum J–R curve in the range of displacement rates of 9.0–90 mm/min for SA508 Gr.1a LAS at 316°C is attributed to the occurrence of DSA.

The monotonic J–R curves of SA312 TP316 SS for different displacement rates are presented in Fig. 5. Fig. 5A shows that the J–R curve of SA312 TP316 SS slightly increased with increasing displacement rate at RT. However, at 316°C, all of the J–R curves were nearly the same regardless of displacement rate, even though the displacement rate varied from 0.9 mm/min to 1,140 mm/min (Fig. 5B). Past investigation showed that the fracture behavior of austenitic SSs has only a slight loading rate dependency at the operating temperature of NPPs [6]. Hence, the present result showed the typical loading rate dependency of austenitic SSs.

It is clear that SA312 TP316 SS showed only a slight effect of loading rate on the fracture behavior under the monotonic loading condition, while SA508 Gr.1a LAS showed a more pronounced loading rate effect at the operating temperature of NPPs. The fracture behavior of SA508 Gr.1a LAS was non-linearly varied with loading rate and the minimum fracture resistance appeared at an intermediate loading rate between the quasistatic and dynamic loading rates. This specific loading rate dependency is related to the DSA characteristics of SA508 Gr.1a LAS at elevated temperatures.

### 3.2. *Cyclic loading condition*

#### 3.2.1. *Effect of compressive load level*

The cyclic J–R fracture toughness tests were conducted at RT and 316°C under various displacement rates and cyclic load ratios. Figs. 6 and 7 present the cyclic J–R curves of SA508 Gr.1a LAS and SA312 TP316 SS, respectively, tested under a quasistatic loading rate. The corresponding monotonic J–R curves are also exhibited in these figures for comparison.

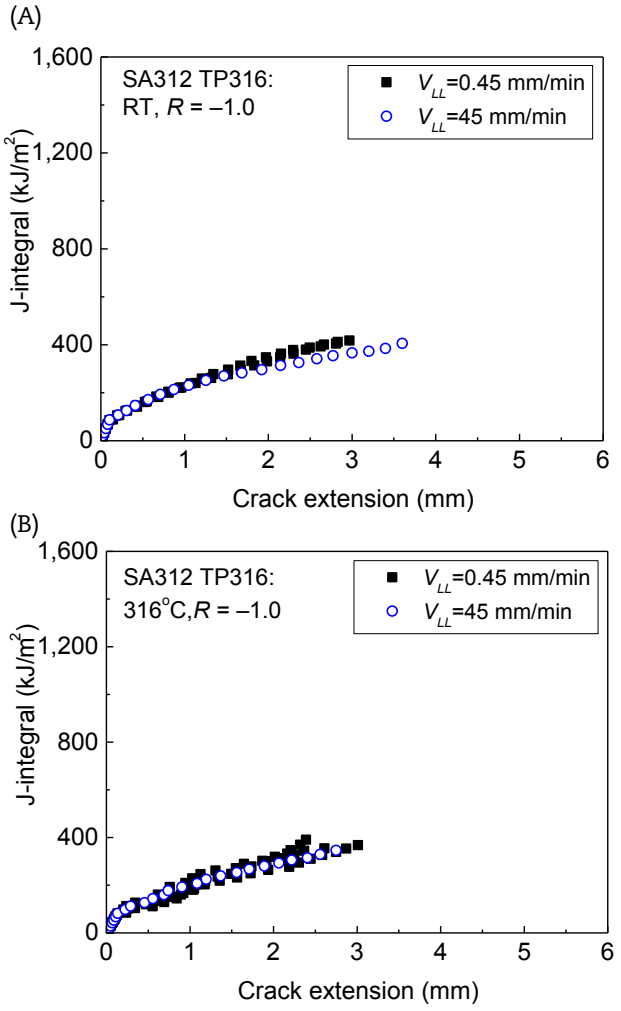


**Fig. 10 – Variation in cyclic *J*–*R* curves of SA312 TP316 SS piping material at different displacement rates. (A) Room temperature, $R = -1.0$. (B) 316°C, $R = -1.0$.**

Regardless of the test temperature and type of material, the cyclic *J*–*R* curves were much lower than their corresponding monotonic *J*–*R* curves. The reduction in the *J*–*R* curves was more significant when the cyclic load ratio was more negative. Such cyclic loading effects were also observed from the results of higher loading rate, although their *J*–*R* curves are not exhibited in the figures. Thus, it is evident that the reversible cyclic load considerably reduced the fracture resistance of the materials regardless of the loading rate, test temperature, and type of material. Several previous studies reported a similar adverse effect of reversible cyclic loading on fracture resistance [6–8,10–12] and they showed that the cyclic effect on fracture resistance saturated when the cyclic load ratio was lower than $R = -1$. Also, microscopic examination near the crack-tip during the tensile and compressive loading steps revealed that the acceleration of the crack extension under a reversible cyclic load was associated with crack-tip sharpening, which developed during the compressive loading step in the cyclic loading [6,10,11]. Thus, the significant reduction in fracture resistance under cyclic loading with higher compressive load related to the enhancement of crack-tip sharpening and the saturation of the cyclic loading effect when $R \leq -1$ was associated with crack faces contacting each other during the compressive loading.

To quantitatively investigate the cyclic loading effect on the fracture resistance, the $J_{1.0\ mm}$ values, which are *J* values at a crack extension of 1.0 mm, for different temperatures and materials are compared in Fig. 8. Fig. 8A presents $J_{1.0\ mm}$ values for tests under the quasistatic loading rate and Fig. 8B shows $J_{1.0\ mm}$ values for $V_{LL} = 2{,}280$ mm/min for SA508 Gr.1a LAS and $V_{LL} = 45$ mm/min for SA312 TP316 SS. Regardless of the loading rate, $J_{1.0\ mm}$ at 316°C were clearly lower than those at RT when a monotonic load and a cyclic load of $R = -0.5$ were applied, but the difference of $J_{1.0\ mm}$ values at RT and 316°C was relatively small when a cyclic load of $R = -1.0$ was applied. Also, comparison of the $J_{1.0\ mm}$ values for both pipe materials showed that the $J_{1.0\ mm}$ values of SA508 Gr.1a LAS were much lower than those of SA312 TP316 SS under a monotonic and cyclic load of $R = -0.5$. However, the $J_{1.0\ mm}$ values for both pipe materials were almost identical under the cyclic load of $R = -1.0$ at both test temperatures. Thus, the fracture behavior was less sensitive to test temperature and type of material at the more negative cyclic load ratio. This is because the contribution to crack extension by the crack-tip sharpening effect under cyclic loading was predominant compared with other parameters when the compressive load level of the cyclic load was high enough to reach the saturated condition of the cyclic effect.

### 3.2.2. *Effect of loading rate*

The *J*–*R* curves of the cyclic tests were compared for different displacement rates to investigate the effect of loading rate on the fracture behavior under the cyclic loading condition. Fig. 9 exhibits the *J*–*R* curves of SA508 Gr.1a LAS tested under cyclic loads of $R = -0.5$ and $-1.0$ at various displacement rates. Figs. 9A and 9B show that the variation in the *J*–*R* curves was negligible at RT for both cyclic load ratios, even if the displacement rate was increased by about 2,300-fold. At 316°C, however, the cyclic *J*–*R* curves varied with the displacement rate; in particular, the variation was pronounced for the cyclic load of $R = -0.5$. For $R = -0.5$, as shown in Fig. 9C, the cyclic *J*–*R* curve at 316°C decreased with increasing displacement rate and showed a minimum at displacement rates in the range of 9.0–90 mm/min. Then, it increased with further increasing displacement rate. Also, for $R = -1$ the displacement rate dependency was similar to that for $R = -0.5$, but the variation in the *J*–*R* curves with displacement rate was insignificant when compared to that for $R = -0.5$ (Fig. 9D). By contrast, as shown in Fig. 10, the cyclic *J*–*R* curves of SA312 TP316 SS, tested under the cyclic load of $R = -1$ at displacement rates of 0.45 mm/min and 45 mm/min, indicated that the fracture resistance was nearly independent of the displacement rate at RT and 316°C. Thus, it was concluded that the effect of the loading rate on the fracture behavior under the cyclic loading condition was negligible for SA312 TP316 SS, regardless of the test temperature. However, the effect was appreciable for SA508 Gr.1a LAS at the operating temperature of NPPs and the minimum in the *J*–*R* curve appeared at an intermediate loading rate, i.e., $V_{LL} = 9.0$–90 mm/min. This indicated that the loading rate effect for both piping materials under the cyclic loading condition was basically the same as that observed under the

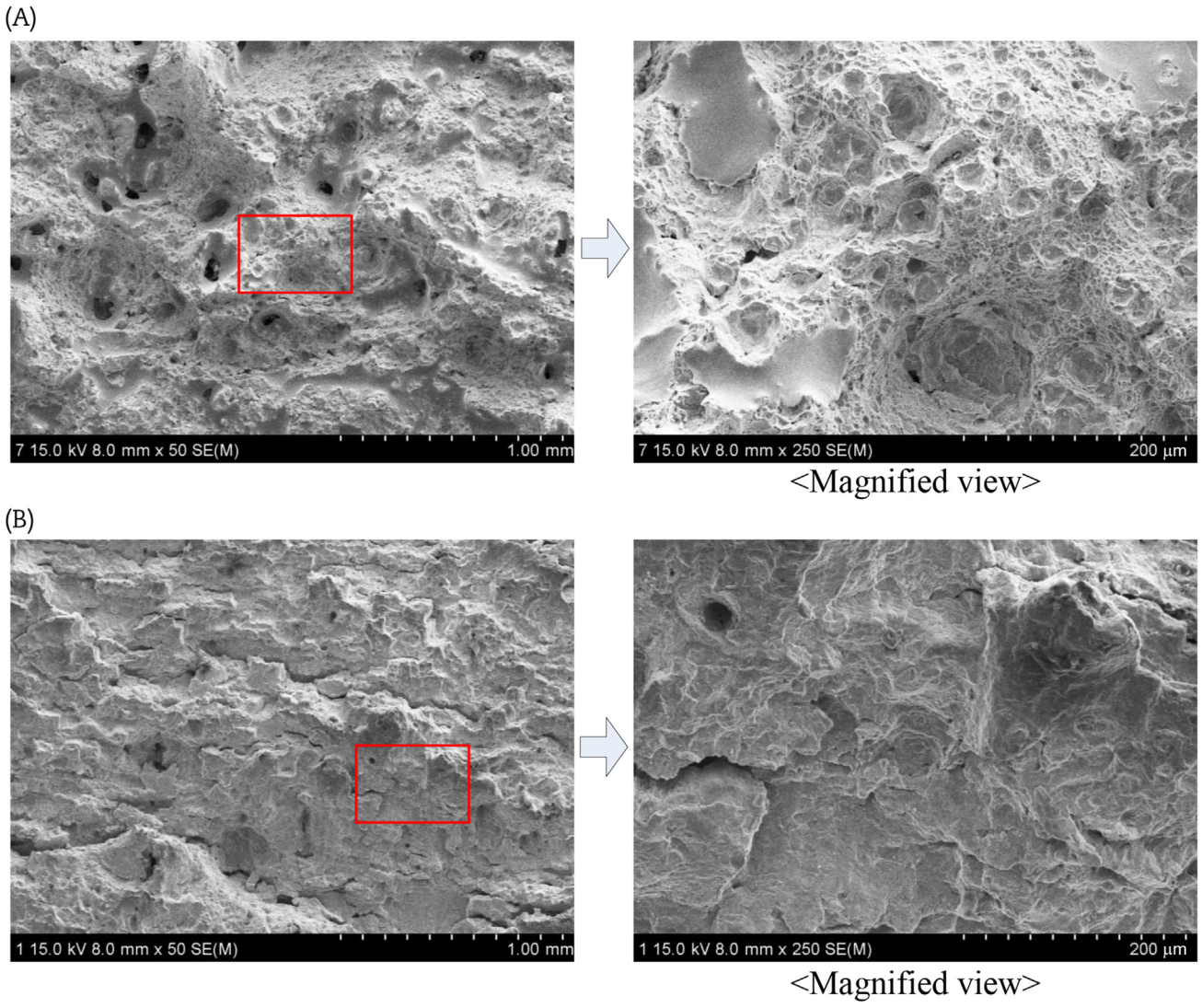


**Fig. 11 – Fracture surfaces of SA508 Gr.1a LAS tested at 316°C under monotonic and cyclic loading conditions. (A) Monotonic load, $V_{LL} = 0.9$ mm/min. (B) Cyclic load of $R = -1.0$, $V_{LL} = 0.9$ mm/min.**

monotonic loading condition. Also, it was evident that, for SA508 Gr.1a LAS, the DSA phenomenon still influenced the loading rate dependency at the operating temperature of NPPs, even under a cyclic load.

Notably, the loading rate effect of SA508 Gr.1a LAS was dependent on the cyclic load ratio; i.e., the loading rate effect was greatly diminished when the cyclic load ratio was −1.0. This was related to the specific crack extension mechanism under the reversible cyclic loading condition. As mentioned in the previous section, the crack extension under a cyclic load is governed by both ductile tearing and crack-tip sharpening mechanisms. It is known that the occurrence of DSA promotes ductile tearing by decreasing the fracture strain near the crack-tip, thereby resulting in degradation of the fracture resistance of ferritic materials [19–21]. Therefore, the influence of DSA clearly appeared for monotonic loading and cyclic loading at $R = -0.5$, where the ductile tearing dominated the crack extension and thus the loading rate effect on fracture behavior was pronounced. However, as the cyclic load ratio became more negative, crack-tip sharpening dominated crack extension. Therefore, the crack-tip sharpening effect on crack extension overshadowed the DSA effect on ductile tearing, so that the loading rate effect because of DSA phenomena was less at $R = -1.0$. The crack-tip sharpening under cyclic load is also indicated from the fracture surfaces of post-test specimens. Fig. 11 presents the fracture surfaces of SA508 Gr.1a LAS tested at 316°C under monotonic load and cyclic load of $R = -1.0$. The fracture surfaces of monotonic loading show dimples, which confirms that ductile tearing is the predominant mechanism of fracture, whereas the cyclic fracture surfaces reveal flat features along with fissure cracks, indicating smearing out of microvoids near the crack-tip due to the contact of crack faces. Thus, it is demonstrated that the crack-tip was closed and sharpened when subjected to compressive load.

### 3.3. *Consideration of seismic loading characteristics in the evaluation of fracture behavior*

Because the seismic load has cyclic and dynamic characteristics, these loading characteristics should be properly

considered in the evaluation of the fracture behavior of pipe materials to assess the integrity of piping components reliably under a seismic condition. The present results indicate that a reversible cyclic load significantly reduces the fracture resistance of the materials and the cyclic effect was dependent on the compressive level of the cyclic load. However, the adverse cyclic effect on the fracture behavior saturated when the cyclic load ratio reached $R = -1$, regardless of the loading rate, test temperature, and type of material. The loading rate effect on the fracture behavior under the cyclic loading condition was negligible for SA312 TP316 SS, while the effect was considerable for SA508 Gr.1a LAS at the operating temperature of NPPs. The fracture resistance of SA508 Gr.1a LAS at 316°C varied nonlinearly with loading rate, and a minimum appeared at an intermediate loading rate. This loading rate effect for SA508 Gr.1a LAS under the cyclic loading condition was diminished when the cyclic load ratio was $R = -1$.

Based on these results, it is therefore suggested that the fracture behavior of pipe materials, which conservatively takes into account the seismic loading characteristics, can be evaluated when testing is done under the reversible cyclic load of $R = -1$ with a quasistatic loading rate, although the seismic load has a cyclic characteristic with random amplitude and various loading rates.

## 4. Conclusions

The effect of loading rate on the fracture behavior under cyclic loading conditions was investigated to understand clearly the fracture behavior of piping materials under seismic conditions. Monotonic and cyclic $J$–$R$ fracture toughness testing of SA508 Gr.1a LAS and SA312 TP316 SS pipe materials were conducted under various displacement rates at RT and 316°C, which is the operating temperature of NPPs. The conclusions of the study are as follows:

1) Regardless of the loading rate, temperature, and type of material, the fracture resistance of the pipe materials under cyclic loading conditions was considerably lower than that under the corresponding monotonic loading condition.
2) The fracture behavior of SA312 TP316 SS was nearly independent of the loading rate under both cyclic and monotonic loading conditions, regardless of the test temperature.
3) The loading rate effect on fracture behavior was appreciable at 316°C for SA508 Gr.1a LAS under both cyclic and monotonic loading conditions. Its fracture resistance nonlinearly varied with loading rate, and the minimum appeared at an intermediate loading rate between the quasistatic and dynamic rates. However, this loading rate dependency was diminished when the cyclic load ratio was $R = -1$.
4) The fracture behavior of the pipe materials, which includes the seismic loading characteristics, can be evaluated when testing is done under the cyclic load of $R = -1$ at a quasistatic loading rate.

## Conflicts of interest

All authors have no conflicts of interest to declare.

## Acknowledgments

This research was supported by the National Research Foundation of Korea (NRF), funded by the Ministry of Science, ICT and Future Planning (NRF–2013M2A8A1040924) and the Nuclear Power Core Technology Development Program of the Korea Institute of Energy Technology Evaluation and Planning (KETEP), granted financial resource from the Ministry of Trade, Industry & Energy, Republic of Korea (20141520100860).

## REFERENCES

[1] ASME, ASME B&PV Code Sec. III, Nuclear Components, 1998.
[2] ASME, ASME B&PV Code Sec. XI, Rules for Inservice Inspection of Nuclear Power Plant Components, 1998.
[3] J.D. Stevenson, Summary of the historical development of seismic design of nuclear power plants in Japan and the U.S. Nucl. Eng. Des 269 (2014) 160–164.
[4] G. Saji, Safety goals for seismic and tsunami risks: lessons learned from the Fukushima Daiichi disaster, Nucl. Eng. Des 280 (2014) 449–463.
[5] USNRC, Evaluation of Potential Pipe Break, NUREG–1061 Vol. 3, 1984.
[6] USNRC, The Effect of Cyclic and Dynamic Loading on the Fracture Resistance of Nuclear Piping Steels, NUREG/CR–6440, 1996.
[7] C.S. Seok, K.L. Murty, A study on the decrease of fracture resistance curve under reversed cyclic loading, Int. J. Pres. Ves. Piping 77 (2000) 303–311.
[8] P.K. Singh, V.R. Ranganath, S. Tarafder, P. Prasad, V. Bhasin, K.K. Vaze, H.S. Kushwaha, Effect of cyclic loading on elastic-plastic fracture resistance of PHT system piping material of PHWR, Int. J. Pres. Ves. Piping 80 (2003) 745–752.
[9] B. Tranchand, S. Chapuliot, V. Aubin, S. Marie, M. Bourgeois, Ductile Fracture Analysis Under Large Amplitude Cycles, Proc. ASME PVP Conf. PVP2014–PVP28426, 2014.
[10] T. Chowdhury, S. Sivaprasad, H.N. Bar, S. Tarafder, N.R. Bandyopadhyay, Cyclic fracture behaviour of 20MnMoNi55 steel at room and elevated temperatures, Fat. Frac. Eng. Mater. Struc 38 (2015) 813–827.
[11] H. Roy, S. Sivaprasad, S. Tarafder, K.K. Ray, Monotonic vis-à-vis cyclic fracture behavior of ANSI 304LN stainless steel, Eng. Frac. Mech 76 (2009) 1822–1832.
[12] S.K. Gupta, V. Bhasin, J. Chattopadhyay, A.K. Ghosh, R.K. Singh, Cyclic-tearing behavior and $J$–$R$ curves of Indian NPP pipes under displacement-controlled cyclic loading, Int. J. Pres. Ves. Piping 132–133 (2015) 72–86.
[13] ASTM, Standard Test Method for Measurement of Fracture Toughness, ASTM E1820-09, 2009.
[14] USNRC, Development of Technical Basis for Leak-Before-Break Procedure, NUREG/CR-6765, 2002.
[15] H.H. Johnson, Calibrating the electric potential method for studying slow crack growth, Mater. Res. Stand 5 (1965) 442–445.
[16] J.A. Joyce, G.E. Sutton, An automated method of computer-controlled low-cycle fatigue crack growth testing using the

elastic–plastic parameter cyclic J, ASTM STP 877 (1985) 227–247.
[17] J.A. Joyce, E.M. Hackett, C. Roe, Effect of cyclic loading on the deformation and elastic-plastic fracture behaviour of cast stainless steel, ASTM STP 1207 (1994) 722–741.
[18] J.W. Kim, M.R. Choi, Effect of loading rate on the deformation behavior of SA508 Gr. 1a low-alloy steel and TP316 stainless steel pipe materials at RT and 316°C, Trans. KSME (A) 39 (2015) 383–390.
[19] USNRC, Effect of Dynamic Strain Aging on the Strength and Toughness of Nuclear Ferritic Piping at LWR Temperatures, NUREG/CR–6226, 1994.
[20] J.W. Kim, I.S. Kim, Investigation of dynamic strain aging on SA106 Gr. C piping steel, Nucl. Eng. Des 172 (1997) 49–59.
[21] J.H. Yoon, B.S. Lee, Y.J. Oh, J.H. Hong, Effects of loading rate and temperature on J–R fracture resistance of an SA516–Gr.70 steel for nuclear piping, Int. J. Pres. Ves. Piping 76 (1999) 663–670.